IOP Publishing Smart Materials and Structures
Smart Mater. Struct. **22** (2013) 094026 (11pp) doi:10.1088/0964-1726/22/9/094026

Analysis of an array of piezoelectric energy harvesters connected in series

H C Lin, P H Wu, I C Lien and Y C Shu[1]

Institute of Applied Mechanics, National Taiwan University, Taipei 106, Taiwan, Republic of China

E-mail: yichung@iam.ntu.edu.tw

Received 27 January 2013, in final form 9 April 2013
Published 27 August 2013
Online at stacks.iop.org/SMS/22/094026

Abstract
This paper investigates the electrical response of a series connection of piezoelectric energy harvesters (PEHs) attached to various interface electronics, including standard and parallel-/series-SSHI (synchronized switch harvesting on inductor) circuits. In contrast to the case of parallel connection of multiple oscillators, the system response is determined by the matrix formulation of charging on a capacitance. In addition, the adoption of an equivalent impedance approach shows that the capacitance matrix can be explicitly expressed in terms of the relevant load impedance. A model problem is proposed for performance evaluation of harvested power under different choices of interface circuits. The result demonstrates that the parallel-SSHI array system exhibits higher power output with moderate bandwidth improvement, while the series-SSHI system delivers a pronounced wideband at the cost of peak harvested power. The standard array system shows a mild ability in power harvesting between these two SSHI systems. Finally, comparisons between the series and parallel connection of oscillators are made, showing the striking contrast of these two cases.

1. Introduction

Piezoelectric energy harvesting based on the resonant vibration of a single piezoelectric oscillator has received significant research attention recently [8, 9, 38–40, 42, 48, 49, 51]. It has many merits over other vibration-to-electricity transduction methods due to the high electromechanical coupling, no requirement for external voltage sources and ease of implementation in tiny devices [6, 17, 23, 35, 36, 41, 43, 54, 61, 63]. As a result, improvements in the use of piezoelectric elements for power harvesting have witnessed a dramatic rise. These include the development of suitable designs of oscillators [1, 7, 15, 18–20, 28, 37, 46, 65] and efficient energy harvesting circuits for power optimization [2, 12, 22, 31, 34, 44, 50, 58, 59].

While this approach has enjoyed great success in many aspects, there are two shortcomings. The first one is the low power area density and the second is the pronounced power reduction at off-resonance. The former is hard to improve due to limitations in the area of devices and the latter requires sophisticated techniques for frequency tuning by developing adjustable stiffness structures [3, 4, 13, 16, 21, 24, 64] or the use of nonlinear techniques [5, 14, 33, 45, 52, 55–57]. This has motivated a prototype based on the use of multiple piezoelectric oscillators, since such a design allows three-dimensional deployment of structures to give increased power area density in a confined space. In addition, the overall bandwidth of an array structure can be enlarged by suitably adjusting the resonance of each oscillator. As a result, numerous research works have described the design of piezoelectric power generators based on the use of multiple oscillators [10, 11, 47, 53, 60, 62]. However, most of these studies replace practical energy harvesting circuits by a resistor, resulting in the neglect of the reaction of interface circuits on the dynamics of the mechanical system [25–27]. The consideration of DC power output in a few other studies lacks sufficient analysis, giving rise to no estimates on harvested power. Hence, there is an urgent need to develop a suitable methodology to study this problem. Indeed, Lien and Shu [29, 30] have recently investigated piezoelectric energy harvesting based on the design of multiple oscillators. They have proposed two approaches to study this problem. One is based on the direct integration of the system equations [29] and the other utilizes the idea of equivalent load impedance [30]. Several analytic estimates on harvested power have been proposed for the

[1] Author to whom any correspondence should be addressed.

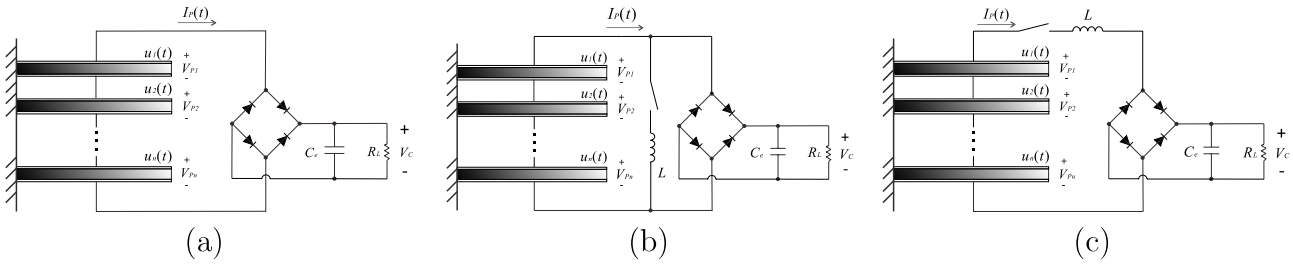

Figure 1. A series connection of an array of piezoelectric energy harvesters attached to the standard interface (a), the parallel-SSHI interface (b), and the series-SSHI interface (c).

parallel connection of a piezoelectric energy harvester (PEH) array structure attached to various energy harvesting circuits, including standard and parallel-/series-SSHI (synchronized switch harvesting on inductor) interfaces. They have shown that the electrical response of a PEH array can be changed from the power-boosting mode to the wideband mode by adjusting the system parameters of each oscillator.

Although the case of parallel connection of multiple piezoelectric oscillators has been investigated in detail [30], there are certain disadvantages in this design. First, the optimal voltage of oscillators connected in parallel is much smaller than that of oscillators connected in series, giving rise to a difficulty in overcoming the forward threshold voltage of diodes under weak levels of excitation. Besides, the optimal impedance of the former is smaller than that of the latter, giving rise to the need to consider electrical loss due to diodes and switches. Thus, there is a need to analyze the latter case. Indeed, here we study the electrical response of a series connection of multiple piezoelectric oscillators attached to various interface circuits, as illustrated in figure 1. The methodology is based on the direct integration of the system equations, including the consideration of balance of charge, energy and electromechanical dynamics. The steady-state response of an array system connected in series is obtained analytically and explained by the equivalent impedance. It is shown that the system response is determined by the matrix formulation of charging on a capacitance. This is very different from the case of parallel connection of a PEH array system, where the system behavior is formulated by the matrix form of the generalized Ohm's law [30]. Finally, the proposed estimates are applied to a model problem in which the performance evaluation is carried out for different energy harvesting circuits. In addition, the results are compared to the case of parallel connection of oscillators, showing an interesting contrast in the electrical response in these two cases.

2. Model

Consider an array of piezoelectric oscillators connected in series, as shown in figure 1. It is assumed that there are no significant differences in the parameters of each piezoelectric oscillator and the modal density of each oscillator is widely separated. Further assume that the structure is vibrating at around the resonance frequency. In this case, the array system can be modeled as a mass + spring + damper + piezostructure, with governing equations described by [30, 48]

$$M_n\ddot{u}_n(t) + \eta_n\dot{u}_n(t) + K_n u_n(t) + \Theta_n V_{\mathrm{p}_n}(t) = F_n(t), \tag{1}$$

$$-\Theta_n\dot{u}_n(t) + C_{\mathrm{p}_n}\dot{V}_{\mathrm{p}_n}(t) = -I_n(t), \tag{2}$$

$$F_n(t) = \bar{F}_n\cos(wt - \tau_n), \tag{3}$$

where $n = 1, 2, \ldots, N$ and N is the total number of oscillators, u_n the displacement of the nth mass M_n, V_{p_n} the voltage across the nth piezoelectric element, $F_n(t)$ the forcing function applied to the nth oscillator and $I_n(t)$ the current flowing into the specified circuit. In addition, in equations (1) and (2), η_n, K_n, Θ_n and C_{p_n} are the mechanical damping coefficient, the stiffness, the piezoelectric coefficient and the capacitance of the nth piezoelectric oscillator. The forcing function $F_n(t)$ is assumed to be harmonic, with w as the angular frequency (in radians per second) and τ_n as the given phase shift angle. However, for a vibrating source with its energy distributed over a wide spectrum of frequencies, the proposed framework is not suitable. Instead, oscillators with nonlinear stiffness have been recently proposed to enhance power extraction under random-frequency excitations [5, 33, 55, 57].

Next, as the array system is connected in series, the overall piezoelectric voltage $V_{\mathrm{p}}(t)$, capacitance C_{p} and current $I_{\mathrm{p}}(t)$ flowing into the specified circuit are

$$V_{\mathrm{p}}(t) = \sum_{n=1}^{N} V_{\mathrm{p}_n}(t), \qquad \frac{1}{C_{\mathrm{p}}} = \sum_{n=1}^{N}\frac{1}{C_{\mathrm{p}_n}}, \qquad I_{\mathrm{p}}(t) = I_{\mathrm{p}_n}(t), \qquad \forall n. \tag{4}$$

In addition, we define

$$V^*_{\mathrm{p}_n}(t) = \frac{\Theta_n}{C_{\mathrm{p}_n}}u_n(t), \qquad V^*_{\mathrm{p}}(t) = \sum_{n=1}^{N} V^*_{\mathrm{p}_n}(t), \tag{5}$$

where $V^*_{\mathrm{p}_n}(t)$ is the equivalent voltage source due to mechanical vibration of the nth oscillator and $V^*_{\mathrm{p}}(t)$ is the overall equivalent voltage source due to vibration of an array of oscillators. Therefore, equation (2) can be rewritten as

$$\dot{V}^*_{\mathrm{p}}(t) = \dot{V}_{\mathrm{p}}(t) + \frac{1}{C_{\mathrm{p}}}I_{\mathrm{p}}(t). \tag{6}$$

Now under the steady-state operation, the displacement of each oscillator is set to be

$$u_n(t) = \bar{u}_n\cos(wt - \tau_n - \theta_n), \tag{7}$$

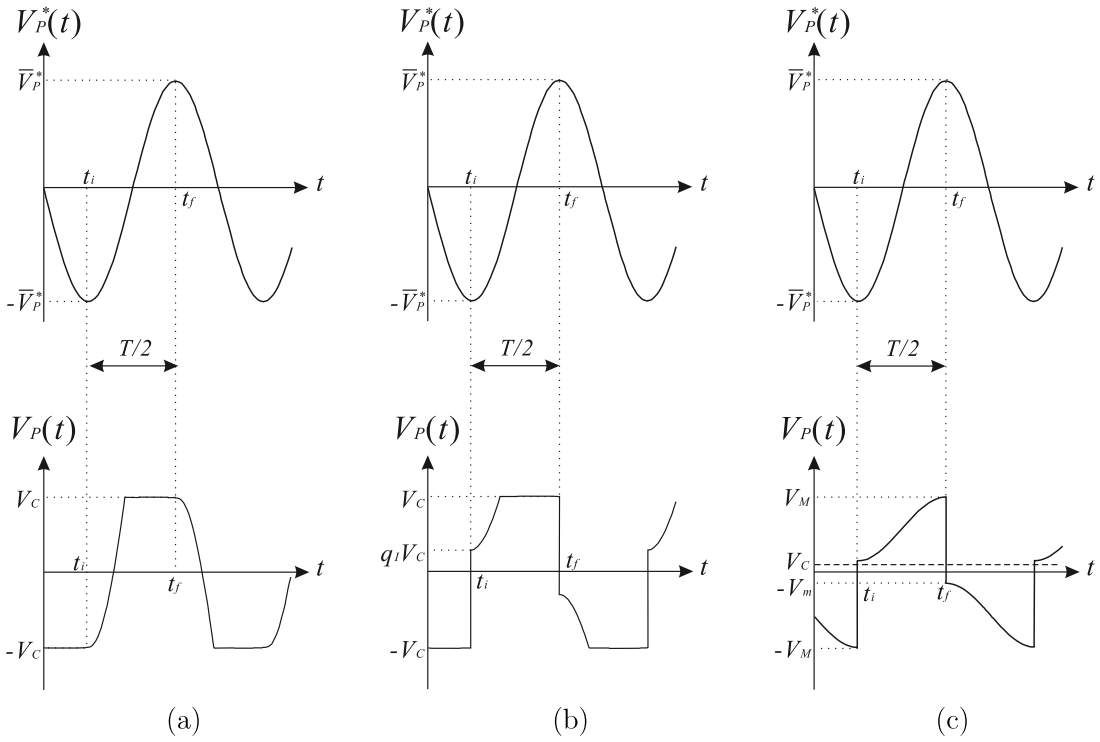

Figure 2. Typical waveforms of the overall equivalent voltage source $V_{\mathrm{p}}^*(t)$ and piezoelectric voltage $V_{\mathrm{p}}(t)$ for the standard interface (a), the parallel-SSHI interface (b), and the series-SSHI interface (c).

where $\bar{u}_n$ is the magnitude of displacement and θ_n is the relative phase shift. Thus, from equation (5), the overall equivalent voltage source due to vibration can be expressed as

$$V_{\mathrm{p}}^*(t) = \bar{V}_{\mathrm{p}}^* \cos(wt - \alpha), \tag{8}$$

where α is the phase shift and $\bar{V}_{\mathrm{p}}^*$ is the magnitude of $V_{\mathrm{p}}^*(t)$ and is related to $\bar{u}_n$ by

$$\bar{V}_{\mathrm{p}}^* = \sum_{n=1}^{N} \frac{\Theta_n}{C_{\mathrm{p}_n}} \bar{u}_n \mathrm{e}^{\mathrm{j}(\alpha-\tau_n-\theta_n)}, \qquad \mathrm{j}^2 = -1. \tag{9}$$

Indeed, the substitution of equation (7) into equation (5) together with equation (8) provides

$$\begin{aligned} & V_{\mathrm{p}}^*(t) \\ &= \sum_{n=1}^{N} [\cos(\tau_n + \theta_n) \cos wt + \sin(\tau_n + \theta_n) \sin wt] \frac{\Theta_n}{C_{\mathrm{p}_n}} \bar{u}_n \\ &= [\cos\alpha \cos wt + \sin\alpha \sin wt] \bar{V}_{\mathrm{p}}^*. \end{aligned}$$

This leads to

$$\cos(-\alpha)\bar{V}_{\mathrm{p}}^* = \sum_{n=1}^{N} \cos(-\tau_n - \theta_n) \frac{\Theta_n}{C_{\mathrm{p}_n}} \bar{u}_n$$

$$\sin(-\alpha)\bar{V}_{\mathrm{p}}^* = \sum_{n=1}^{N} \sin(-\tau_n - \theta_n) \frac{\Theta_n}{C_{\mathrm{p}_n}} \bar{u}_n$$

which in turn gives the desired result of equation (9).

2.1. Standard circuit

Suppose the array of oscillators is connected to a standard circuit consisting of a rectifier followed by a filtering capacitance C_{e} for AC/DC conversion, as shown in figure 1(a). The terminal load is represented by a resistor R_{L} and V_{c} is the DC voltage across it, as also shown in figure 1(a). The rectifying bridge is assumed to be perfect here. Under the steady-state excitation of a single signal, the typical waveforms of the equivalent voltage source $V_{\mathrm{p}}^*(t)$ and overall piezoelectric voltage $V_{\mathrm{p}}(t)$ are shown schematically in figure 2(a).

Now let t_{i} and t_{f} be two time instants such that $V_{\mathrm{p}}^*(t)$ goes from the minimum $-\bar{V}_{\mathrm{p}}^*$ to the maximum $+\bar{V}_{\mathrm{p}}^*$, as shown in figure 2(a). Let T denote the period of mechanical excitation. Hence, $\frac{T}{2} = \frac{\pi}{w} = t_{\mathrm{f}} - t_{\mathrm{i}}$. From the principle of balance of charge conservation, we have

$$\int_{t_{\mathrm{i}}}^{t_{\mathrm{f}}} I_{\mathrm{p}}(t)\,\mathrm{d}t = \frac{T}{2}\frac{V_{\mathrm{c}}}{R_{\mathrm{L}}} = \frac{\pi}{w}\frac{V_{\mathrm{c}}}{R_{\mathrm{L}}}. \tag{10}$$

Thus, the integration of equation (6) from t_{i} to t_{f} gives

$$2\bar{V}_{\mathrm{p}}^* = 2V_{\mathrm{c}} + \frac{1}{C_{\mathrm{p}}}\frac{\pi}{w}\frac{V_{\mathrm{c}}}{R_{\mathrm{L}}}. \tag{11}$$

This gives the relation between the DC voltage V_{c} and the magnitude of overall equivalent voltage source $\bar{V}_{\mathrm{p}}^*$ as

$$V_{\mathrm{c}}^{\mathrm{Standard}} = \left(\frac{C_{\mathrm{p}} w R_{\mathrm{L}}}{\frac{\pi}{2} + C_{\mathrm{p}} w R_{\mathrm{L}}}\right) \bar{V}_{\mathrm{p}}^*. \tag{12}$$

Next, the use of equation (2) to eliminate V_{p_n} from equation (1) gives

$$M_n\frac{\mathrm{d}}{\mathrm{d}t}\ddot{u}_n(t)+\eta_n\frac{\mathrm{d}}{\mathrm{d}t}\dot{u}_n(t)+K_n\frac{\mathrm{d}}{\mathrm{d}t}u_n(t)+\frac{\Theta_n^2}{C_{\mathrm{p}_n}}\dot{u}_n(t) - \frac{\Theta_n}{C_{\mathrm{p}_n}}I_{\mathrm{p}}(t)=\frac{\mathrm{d}}{\mathrm{d}t}F_n(t). \tag{13}$$

By using equations (7), (10) and (12), the integration of equation (13) over the half-cycle from t_{i} to t_{f} provides

$$\begin{aligned}\bar{F}_n\cos(\alpha-\tau_n)=&\frac{-\pi}{2}\frac{\Theta_n}{C_{\mathrm{p}_n}}\left(\frac{C_{\mathrm{p}}}{\frac{\pi}{2}+C_{\mathrm{p}}wR_{\mathrm{L}}}\right)\bar{V}_{\mathrm{p}}^*\\&+\left[\left(K_n-w^2M_n+\frac{\Theta_n^2}{C_{\mathrm{p}_n}}\right)\right.\\&\times\cos(\alpha-\tau_n-\theta_n)-\eta_nw\\&\left.\times\sin(\alpha-\tau_n-\theta_n)\right]\bar{u}_n.\end{aligned} \tag{14}$$

Finally, we consider the formulation from the principle of balance of energy. However, different from the case of parallel connection of the PEH array, where equation (1) is multiplied by current for the consideration of energy balance, here we consider a different formulation. Indeed, we first eliminate V_{p_n} from equation (1) by using equation (2) and multiply equation (1) by $\dot{V}_{\mathrm{p}}^*(t)$. This gives

$$\int_{t_{\mathrm{i}}}^{t_{\mathrm{f}}}\left(M_n\ddot{u}_n(t)+\eta_n\dot{u}_n(t)+K_nu_n(t)+\frac{\Theta_n^2}{C_{\mathrm{p}_n}}u_n(t) +\frac{\Theta_n}{C_{\mathrm{p}_n}}Q_{\mathrm{p}}(t)-F_n(t)\right)\dot{V}_{\mathrm{p}}^*(t)\,\mathrm{d}t=0, \tag{15}$$

where $Q_{\mathrm{p}}=Q_{\mathrm{p}_n}$ and $I_{\mathrm{p}}(t)=-\frac{\mathrm{d}}{\mathrm{d}t}Q_{\mathrm{p}}(t)$ due to the characteristics of series connection of piezoelectric oscillators. Next, the balance of energy gives [48, 49]

$$\int_{t_{\mathrm{i}}}^{t_{\mathrm{f}}}I_{\mathrm{p}}(t)V_{\mathrm{p}}(t)\,\mathrm{d}t=\frac{\pi}{w}\frac{V_{\mathrm{c}}^2}{R_{\mathrm{L}}} \tag{16}$$

and the repeated use of equation (6) provides

$$\begin{aligned}&\frac{1}{C_{\mathrm{p}}}\int_{t_{\mathrm{i}}}^{t_{\mathrm{f}}}\dot{V}_{\mathrm{p}}^*(t)Q_{\mathrm{p}}(t)\,\mathrm{d}t\\&=\int_{t_{\mathrm{i}}}^{t_{\mathrm{f}}}\dot{V}_{\mathrm{p}}^*(t)V_{\mathrm{p}}(t)\,\mathrm{d}t-\int_{t_{\mathrm{i}}}^{t_{\mathrm{f}}}\dot{V}_{\mathrm{p}}^*(t)V_{\mathrm{p}}^*(t)\,\mathrm{d}t\\&=\int_{t_{\mathrm{i}}}^{t_{\mathrm{f}}}\left(\dot{V}_{\mathrm{p}}(t)+\frac{1}{C_{\mathrm{p}}}I_{\mathrm{p}}(t)\right)V_{\mathrm{p}}(t)\,\mathrm{d}t-\frac{1}{2}\left[V_{\mathrm{p}}^*(t)\right]^2\Big|_{t_{\mathrm{i}}}^{t_{\mathrm{f}}}\\&=\frac{1}{2}\left[V_{\mathrm{p}}(t)\right]^2\Big|_{t_{\mathrm{i}}}^{t_{\mathrm{f}}}+\frac{1}{C_{\mathrm{p}}}\left(\frac{\pi}{w}\frac{V_{\mathrm{c}}^2}{R_{\mathrm{L}}}\right)-\frac{1}{2}\left[(\bar{V}_{\mathrm{p}}^*)^2-(-\bar{V}_{\mathrm{p}}^*)^2\right]\\&=\frac{1}{2}\left[(V_{\mathrm{c}})^2-(-V_{\mathrm{c}})^2\right]+\left(\frac{\pi}{C_{\mathrm{p}}wR_{\mathrm{L}}}\right)V_{\mathrm{c}}^2\\&=\left(\frac{\pi}{C_{\mathrm{p}}wR_{\mathrm{L}}}\right)V_{\mathrm{c}}^2\end{aligned} \tag{17}$$

by observing the waveforms of $V_{\mathrm{p}}^*(t)$ and $V_{\mathrm{p}}(t)$ in figure 2(a). Now substituting equations (7) and (8) into equation (15) together with the aid of equations (12) and (17) provides

$$\begin{aligned}\bar{F}_n\sin(\alpha-\tau_n)=&\frac{\Theta_n}{C_{\mathrm{p}_n}}\frac{2C_{\mathrm{p}}^2wR_{\mathrm{L}}}{\left(\frac{\pi}{2}+C_{\mathrm{p}}wR_{\mathrm{L}}\right)^2}\bar{V}_{\mathrm{p}}^*\\&+\left[\left(K_n-w^2M_n+\frac{\Theta_n^2}{C_{\mathrm{p}_n}}\right)\right.\\&\times\sin(\alpha-\tau_n-\theta_n)+\eta_nw\\&\left.\times\cos(\alpha-\tau_n-\theta_n)\right]\bar{u}_n.\end{aligned} \tag{18}$$

The magnitude of displacement of each oscillator is then obtained by the simplification of equations (9), (14) and (18). This gives

$$\begin{aligned}\hat{F}_n=&\left[\left(\frac{C_{\mathrm{p}_n}}{\Theta_n}\right)^2\left(K_n-w^2M_n+\mathrm{j}w\eta_n\right)+C_{\mathrm{p}_n}\right]\hat{u}_n\\&+\left[-\frac{\pi}{2}\frac{C_{\mathrm{p}}}{\left(\frac{\pi}{2}+C_{\mathrm{p}}wR_{\mathrm{L}}\right)}+\mathrm{j}\frac{2C_{\mathrm{p}}^2wR_{\mathrm{L}}}{\left(\frac{\pi}{2}+C_{\mathrm{p}}wR_{\mathrm{L}}\right)^2}\right]\\&\times\left(\sum_{k=1}^{N}\hat{u}_k\right),\end{aligned} \tag{19}$$

where

$$\hat{F}_n=\frac{C_{\mathrm{p}_n}}{\Theta_n}\bar{F}_n\mathrm{e}^{\mathrm{j}(\alpha-\tau_n)},\qquad \hat{u}_n=\frac{\Theta_n}{C_{\mathrm{p}_n}}\bar{u}_n\mathrm{e}^{\mathrm{j}(\alpha-\tau_n-\theta_n)}. \tag{20}$$

The explanation of equation (19) will be furnished in section 3.

2.2. *Parallel-SSHI circuit*

Suppose a series connection of a PEH array is connected to another interface circuit, parallel-SSHI, as shown in figure 1(b) [12, 50]. In this case, a switching device and an inductor L are added in parallel between the array and the rectifier. Unlike the case of a single oscillator, in which the switch is triggered when the displacement reaches its extreme values, here the switch is triggered at the extremes of the overall equivalent voltage source $V_{\mathrm{p}}^*(t)$. In addition, the switch stays closed for a time very much shorter than the period of excitation; i.e., $\Delta t=\pi\sqrt{LC_{\mathrm{p}}}\ll\frac{T}{2}=\frac{\pi}{w}$. Therefore, the overall capacitance C_{p} and the inductor L are able to form an electric oscillation to transfer energy within Δt. As a result of electric oscillation, this leads to the inversion of $V_{\mathrm{p}}(t)$ at the extreme values of $V_{\mathrm{p}}^*(t)$, giving rise to a 90° phase shift between these two, as illustrated in figure 2(b). Note that the voltage inversion is not perfect because of energy loss from the inductor in series with the switch. Hence, letting $t_{\mathrm{i}}^+=t_{\mathrm{i}}+\Delta t$, we have

$$V_{\mathrm{p}}(t_{\mathrm{i}}^+)=q_{\mathrm{I}}V_{\mathrm{c}},\qquad q_{\mathrm{I}}=\mathrm{e}^{-\frac{\pi}{2Q_{\mathrm{I}}}}, \tag{21}$$

where Q_{I} is the inversion quality factor. Such an imperfect inversion is also shown in figure 2(b).

From the balance of charge conservation, integrating equation (6) from t_{i}^+ to t_{f} gives

$$2\bar{V}_{\mathrm{p}}^*=(V_{\mathrm{c}}-q_{\mathrm{I}}V_{\mathrm{c}})+\frac{1}{C_{\mathrm{p}}}\frac{\pi}{w}\frac{V_{\mathrm{c}}}{R_{\mathrm{L}}}.$$

Thus, the relation between the magnitude of the overall equivalent voltage source $\bar{V}_{\rm p}^*$ and the rectified voltage $V_{\rm c}$ is

$$V_{\rm c}^{\text{P-SSHI}} = \left(\frac{C_{\rm p} w R_{\rm L}}{\frac{\pi}{2} + \left(\frac{1-q_{\rm I}}{2}\right) C_{\rm p} w R_{\rm L}} \right) \bar{V}_{\rm p}^*. \tag{22}$$

Next, integrating equation (13) for the formulation of the electromechanical dynamics from $t_{\rm i}^+$ to $t_{\rm f}$ gives

$$\begin{aligned} \bar{F}_n \cos(\alpha - \tau_n) = {} & \frac{-\pi}{2} \frac{\Theta_n}{C_{{\rm p}_n}} \left[\frac{C_{\rm p}}{\frac{\pi}{2} + \left(\frac{1-q_{\rm I}}{2}\right) C_{\rm p} w R_{\rm L}} \right] \bar{V}_{\rm p}^* \\ & + \left[\left(K_n - w^2 M_n + \frac{\Theta_n^2}{C_{{\rm p}_n}} \right) \right. \\ & \times \cos(\alpha - \tau_n - \theta_n) - \eta_n w \\ & \left. \times \sin(\alpha - \tau_n - \theta_n) \right] \bar{u}_n. \end{aligned} \tag{23}$$

Finally, consider the formulation of the generalized balance of energy given by equation (15). Different from the result of equation (17), here

$$\begin{aligned} & \frac{1}{C_{\rm p}} \int_{t_{\rm i}^+}^{t_{\rm f}} \dot{V}_{\rm p}^*(t) Q_{\rm p}(t)\, {\rm d}t \\ & = \int_{t_{\rm i}^+}^{t_{\rm f}} \dot{V}_{\rm p}^*(t) V_{\rm p}(t)\, {\rm d}t - \int_{t_{\rm i}^+}^{t_{\rm f}} \dot{V}_{\rm p}^*(t) V_{\rm p}^*(t)\, {\rm d}t \\ & = \int_{t_{\rm i}^+}^{t_{\rm f}} \left(\dot{V}_{\rm p}(t) + \frac{1}{C_{\rm p}} I_{\rm p}(t) \right) V_{\rm p}(t)\, {\rm d}t - \frac{1}{2} \left[V_{\rm p}^*(t) \right]^2 \Big|_{t_{\rm i}^+}^{t_{\rm f}} \\ & = \frac{1}{2} \left[V_{\rm p}(t) \right]^2 \Big|_{t_{\rm i}^+}^{t_{\rm f}} + \frac{1}{C_{\rm p}} \left(\frac{\pi}{w} \frac{V_{\rm c}^2}{R_{\rm L}} \right) - \frac{1}{2} \left[(\bar{V}_{\rm p}^*)^2 - (-\bar{V}_{\rm p}^*)^2 \right] \\ & = \frac{1}{2} \left(1 - q_{\rm I}^2 \right) V_{\rm c}^2 + \left(\frac{\pi}{C_{\rm p} w R_{\rm L}} \right) V_{\rm c}^2 \end{aligned} \tag{24}$$

from the observation of the waveforms of $V_{\rm p}^*(t)$ and $V_{\rm p}(t)$ in figure 2(b). Now substituting equations (7) and (8) into (15), where the integration period is from $t_{\rm i}^+$ to $t_{\rm f}$, we have

$$\begin{aligned} & \bar{F}_n \sin(\alpha - \tau_n) \\ & = \frac{\Theta_n}{C_{{\rm p}_n}} \frac{\left[2 + \left(\frac{1-q_{\rm I}^2}{\pi} \right) C_{\rm p} w R_{\rm L} \right] C_{\rm p}^2 w R_{\rm L}}{\left[\frac{\pi}{2} + \left(\frac{1-q_{\rm I}}{2} \right) C_{\rm p} w R_{\rm L} \right]^2} \bar{V}_{\rm p}^* \\ & \quad + \left[\left(K_n - w^2 M_n + \frac{\Theta_n^2}{C_{{\rm p}_n}} \right) \sin(\alpha - \tau_n - \theta_n) \right. \\ & \quad \left. + \eta_n w \cos(\alpha - \tau_n - \theta_n) \right] \bar{u}_n \end{aligned} \tag{25}$$

with the help of equations (22) and (24).

The magnitude of displacement of each oscillator is then obtained by the simplification of equations (9), (23) and (25). This gives

$$\begin{aligned} \hat{F}_n = {} & \left[\left(\frac{C_{{\rm p}_n}}{\Theta_n} \right)^2 \left(K_n - w^2 M_n + {\rm j} w \eta_n \right) + C_{{\rm p}_n} \right] \hat{u}_n \\ & + \left\{ \frac{-\pi C_{\rm p}}{\left[\pi + (1 - q_{\rm I}) C_{\rm p} w R_{\rm L} \right]} \right. \\ & \left. + {\rm j} \frac{4 \left[2 + \left(\frac{1-q_{\rm I}^2}{\pi} \right) C_{\rm p} w R_{\rm L} \right] C_{\rm p}^2 w R_{\rm L}}{\left[\pi + (1 - q_{\rm I}) C_{\rm p} w R_{\rm L} \right]^2} \right\} \\ & \times \left(\sum_{k=1}^{N} \hat{u}_k \right), \end{aligned} \tag{26}$$

where $\hat{F}_n$ and $\hat{u}_n$ are defined by equation (20).

2.3. Series-SSHI circuit

We now turn to the final case of implementing a series-SSHI interface to a series connection of a PEH array. In this case, a switching device and an inductor are connected to the array structure in series, as shown in figure 1(c) [2, 31]. The switch is set to be triggered at the extreme values of the equivalent voltage source $V_{\rm p}^*(t)$, giving rise to locking of a 90° phase shift angle between $V_{\rm p}^*(t)$ and $V_{\rm p}(t)$. Note that once the switch turns off, the array is in an open-circuit condition, leaving no current flowing out of it. But when the switch is on at time instant $t_{\rm i}$, the overall piezoelectric voltage $V_{\rm p}(t_{\rm i}) = -V_{\rm M}$ is reversed to $V_{\rm p}(t_{\rm i}^+) = V_{\rm m}$ during the inversion process, where $t_{\rm i}^+ - t_{\rm i} = \Delta t = \pi\sqrt{LC_{\rm p}} \ll \frac{\pi}{w}$. From these observations, the typical waveforms of $V_{\rm p}^*(t)$ and $V_{\rm p}(t)$ are shown in figure 2(c). Finally, the electrical oscillation of this switching device gives [2, 31]

$$-(V_{\rm M} - V_{\rm c}) q_{\rm I} = -(V_{\rm M} - V_{\rm c}) {\rm e}^{\frac{-\pi}{2Q_{\rm I}}} = -V_{\rm m} - V_{\rm c}, \tag{27}$$

where $q_{\rm I}$ is defined by equation (21), with $Q_{\rm I}$ as the inversion quality factor due to electric loss in the switching process.

To analyze the electrical response of this array system, first note that from the balance of charge conservation during the inversion process,

$$\Delta Q = C_{\rm p} \Delta V_{\rm p} = C_{\rm p} (V_{\rm M} + V_{\rm m}) = \frac{T}{2} \frac{V_{\rm c}}{R_{\rm L}} = \frac{\pi}{w} \frac{V_{\rm c}}{R_{\rm L}}. \tag{28}$$

Next, integrating equation (6) from $t_{\rm i}^+$ to $t_{\rm f}$ gives

$$2\bar{V}_{\rm p}^* = V_{\rm M} - V_{\rm m} \tag{29}$$

since $I_{\rm p}(t) = 0$ within the time interval $(t_{\rm i}^+, t_{\rm f})$. Thus, from equations (27)–(29), we have

$$\begin{aligned} V_{\rm M} &= \frac{2}{1 - q_{\rm I}} \bar{V}_{\rm p}^* - \left(\frac{1 + q_{\rm I}}{1 - q_{\rm I}} \right) V_{\rm c}, \\ V_{\rm m} &= \frac{2 q_{\rm I}}{1 - q_{\rm I}} \bar{V}_{\rm p}^* - \left(\frac{1 + q_{\rm I}}{1 - q_{\rm I}} \right) V_{\rm c}, \\ V_{\rm c}^{\text{S-SSHI}} &= \frac{2(1 + q_{\rm I}) C_{\rm p} w R_{\rm L}}{(1 - q_{\rm I})\pi + 2(1 + q_{\rm I}) C_{\rm p} w R_{\rm L}} \bar{V}_{\rm p}^*. \end{aligned} \tag{30}$$

Now integrating equation (13) for the formulation of the electromechanical dynamics from $t_{\rm i}^+$ to $t_{\rm f}$ gives

$$\bar{F}_n \cos(\alpha - \tau_n) = \left[\left(K_n - w^2 M_n + \frac{\Theta_n^2}{C_{{\rm p}_n}}\right) \times \cos(\alpha - \tau_n - \theta_n) - \eta_n w \times \sin(\alpha - \tau_n - \theta_n)\right] \bar{u}_n. \tag{31}$$

Finally, consider the generalized balance of the energy formulation in equation (15). Different from the previous two cases, here

$$\begin{aligned}
&\frac{1}{C_{\rm p}} \int_{t_{\rm i}^+}^{t_{\rm f}} \dot{V}_{\rm p}^*(t) Q_{\rm p}(t)\, {\rm d}t \\
&= \int_{t_{\rm i}^+}^{t_{\rm f}} \dot{V}_{\rm p}^*(t) V_{\rm p}(t)\, {\rm d}t - \int_{t_{\rm i}^+}^{t_{\rm f}} \dot{V}_{\rm p}^*(t) V_{\rm p}^*(t)\, {\rm d}t \\
&= \int_{t_{\rm i}^+}^{t_{\rm f}} \left(\dot{V}_{\rm p}(t) + \frac{1}{C_{\rm p}} I_{\rm p}(t)\right) V_{\rm p}(t)\, {\rm d}t - \frac{1}{2}\left[V_{\rm p}^*(t)\right]^2 \Big|_{t_{\rm i}^+}^{t_{\rm f}} \\
&= \tfrac{1}{2}\left[V_{\rm p}(t)\right]^2 |_{t_{\rm i}^+}^{t_{\rm f}} + 0 - \tfrac{1}{2}\left[(\bar{V}_{\rm p}^*)^2 - (-\bar{V}_{\rm p}^*)^2\right] \\
&= \tfrac{1}{2}\left(V_{\rm M}^2 - V_{\rm m}^2\right)
\end{aligned} \tag{32}$$

by observing the waveforms of $V_{\rm p}^*(t)$ and $V_{\rm p}(t)$ in figure 2(c). The substitution of equations (7) and (8) into (15), where the integration period is from $t_{\rm i}^+$ to $t_{\rm f}$ gives

$$\begin{aligned}
&\bar{F}_n \sin(\alpha - \tau_n) \\
&= \frac{\Theta_n}{C_{{\rm p}_n}} \left[\frac{4(1+q_{\rm I})C_{\rm p}}{\left[\pi(1-q_{\rm I}) + 2(1+q_{\rm I})\, C_{\rm p} w R_{\rm L}\right]}\right] \bar{V}_{\rm p}^* \\
&\quad + \left[\left(K_n - w^2 M_n + \frac{\Theta_n^2}{C_{{\rm p}_n}}\right) \sin(\alpha - \tau_n - \theta_n) \right. \\
&\quad \left. + \eta_n w \cos(\alpha - \tau_n - \theta_n)\right] \bar{u}_n
\end{aligned} \tag{33}$$

with the aid of equations (30) and (32).

The magnitude of displacement of each oscillator is then obtained by the simplification of equations (9), (31) and (33), therefore,

$$\begin{aligned}
\hat{F}_n = &\left[\left(\frac{C_{{\rm p}_n}}{\Theta_n}\right)^2 \left(K_n - w^2 M_n + {\rm j} w \eta_n\right) + C_{{\rm p}_n}\right] \hat{u}_n \\
&+ {\rm j}\left[\frac{4(1+q_{\rm I})C_{\rm p}}{\left[(1-q_{\rm I})\pi + 2(1+q_{\rm I})\, C_{\rm p} w R_{\rm L}\right]}\right] \\
&\times \left(\sum_{k=1}^{N} \hat{u}_k\right),
\end{aligned} \tag{34}$$

where $\hat{F}_n$ and $\hat{u}_n$ are defined by equation (20).

3. Interpretation as an equivalent impedance

The results obtained from section 2 can also be explained using the concept of an equivalent impedance, and we use the case of a standard circuit to illustrate it in terms of space saving. From equation (6), the circuit model of a series connection of a PEH array is schematically shown at the top of figure 3. Now let Z be the equivalent impedance of the circuit elements consisting of the piezoelectric capacitance $C_{\rm p}$ and the harvesting circuit, as also illustrated at the bottom of figure 3. Therefore, from Kirchhoff's circuit law,

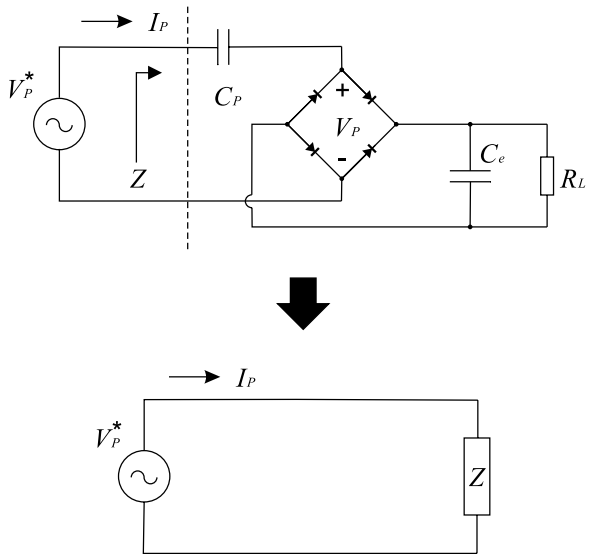

Figure 3. (Top) Equivalent circuit model of a series connection of a PEH array endowed with a standard circuit. (Bottom) Replacing the piezoelectric capacitance and the energy harvesting circuit of the previous circuit model by an equivalent impedance Z.

$$\bar{V}_{\rm p}^* = \bar{I}_{\rm p} Z, \tag{35}$$

where $\bar{I}_{\rm p}$ is the complex magnitude of $I_{\rm p}(t)$. The substitution of equations (7)–(9) and equation (35) into (13) gives

$$\begin{aligned}
&\left[\left(\frac{C_{{\rm p}_n}}{\Theta_n}\right)^2 \left(K_n - w^2 M_n + {\rm j} w \eta_n\right) + C_{{\rm p}_n}\right] \hat{u}_n \\
&\quad - \frac{1}{{\rm j} w Z}\left(\sum_{k=1}^{N} \hat{u}_k\right) = \hat{F}_n,
\end{aligned} \tag{36}$$

where $\hat{F}_n$ and $\hat{u}_n$ are defined by equation (20). Note that equation (36) can be rewritten in the matrix form as

$$\mathbf{Q} = \mathbf{C}\mathbf{V}, \qquad \mathbf{Q} = \{\hat{F}_n\}, \quad \mathbf{V} = \{\hat{u}_n\}, \tag{37}$$

and the matrix $\mathbf{C} = \{C_{mn}\}$ is defined by

$$C_{mn} = \begin{cases} C_{\rm I} & \text{if } m \neq n, \\ C_{\rm O}^{(n)} + C_{\rm I} & \text{if } m = n, \end{cases} \tag{38}$$

where $C_{\rm I}$ is related to the types of interface circuit and $C_{\rm O}^{(n)}$ is associated with the properties of oscillators. They are given by

$$C_{\rm I} = -\frac{1}{{\rm j} w Z}, \tag{39}$$

$$C_{\rm O}^{(n)} = \left(\frac{C_{{\rm p}_n}}{\Theta_n}\right)^2 \left(K_n - w^2 M_n + {\rm j} w \eta_n\right) + C_{{\rm p}_n}. \tag{40}$$

Table 1. Input data used for numerical validation.

	M_n (kg)	η_n (N s m^{-1})	K_n (N m^{-1})	Θ_n (N V^{-1})	C_{p_n} (nF)	F_n (N)
Oscillator 1	0.009 73	0.073 16	786.319	0.001 22	25.78	0.050
Oscillator 2	0.008 95	0.076 82	762.730	0.001 34	26.81	0.051
Oscillator 3	0.010 22	0.074 62	786.319	0.001 28	24.49	0.049

However, the equivalent impedance Z is still unknown. To determine it, consider the case of a single energy harvester; i.e., $N = 1$. In this case, equation (36) is simplified to

$$\frac{\bar{F}}{\bar{u}} = \left\{ \left(K - w^2 M + \frac{\Theta^2}{C_\mathrm{p}} + \frac{\Theta^2}{C_\mathrm{p}^2 w} \hat{Z}_\mathrm{I} \right)^2 + \left(w\eta + \frac{\Theta^2}{C_\mathrm{p}^2 w} \hat{Z}_\mathrm{R} \right)^2 \right\}^{\frac{1}{2}}, \tag{41}$$

where both $\hat{Z}_\mathrm{R}$ and $\hat{Z}_\mathrm{I}$ are defined by

$$\frac{1}{Z} = \hat{Z}_\mathrm{R} - \mathrm{j}\hat{Z}_\mathrm{I}. \tag{42}$$

Note that in this case the analytic steady-state solution of a piezoelectric oscillator connected to the standard interface has been proposed by Shu and Lien (equation (28) in [48]) and is given by

$$\frac{\bar{F}}{\bar{u}} = \left\{ \left(K - w^2 M + \frac{w\Theta^2 R_\mathrm{L}}{\frac{\pi}{2} + C_\mathrm{p} w R_\mathrm{L}} \right)^2 + \left(w\eta + \frac{2w\Theta^2 R_\mathrm{L}}{\left(\frac{\pi}{2} + C_\mathrm{p} w R_\mathrm{L}\right)^2} \right)^2 \right\}^{\frac{1}{2}}. \tag{43}$$

Thus, the comparison between equations (41) and (43) gives

$$\hat{Z}_\mathrm{R}^{\mathrm{Standard}} = \frac{2C_\mathrm{p}^2 w^2 R_\mathrm{L}}{\left(\frac{\pi}{2} + C_\mathrm{p} w R_\mathrm{L}\right)^2}, \qquad \hat{Z}_\mathrm{I}^{\mathrm{Standard}} = \frac{-\pi C_\mathrm{p} w}{2\left(\frac{\pi}{2} + C_\mathrm{p} w R_\mathrm{L}\right)}. \tag{44}$$

In fact, from the approach proposed in section 2.1, the comparison between equations (19) and (36) gives the same load impedance Z as in equation (44). In addition, using an approach similar to the case of the standard circuit, it can be shown that

$$\hat{Z}_\mathrm{R}^{\mathrm{P\text{-}SSHI}} = \frac{4\left[2 + \left(\frac{1-q_\mathrm{I}^2}{\pi}\right) C_\mathrm{p} w R_\mathrm{L}\right] C_\mathrm{p}^2 w^2 R_\mathrm{L}}{\left[\pi + (1 - q_\mathrm{I}) C_\mathrm{p} w R_\mathrm{L}\right]^2}, \qquad \hat{Z}_\mathrm{I}^{\mathrm{P\text{-}SSHI}} = \frac{-\pi C_\mathrm{p} w}{\left[\pi + (1 - q_\mathrm{I}) C_\mathrm{p} w R_\mathrm{L}\right]} \tag{45}$$

for the case of a parallel-SSHI interface and

$$\hat{Z}_\mathrm{R}^{\mathrm{S\text{-}SSHI}} = \frac{4(1 + q_\mathrm{I}) C_\mathrm{p} w}{\left[(1 - q_\mathrm{I})\pi + 2(1 + q_\mathrm{I}) C_\mathrm{p} w R_\mathrm{L}\right]}, \qquad \hat{Z}_\mathrm{I}^{\mathrm{S\text{-}SSHI}} = 0 \tag{46}$$

for the case of a series-SSHI interface.

Finally, equation (37) is a matrix formulation for charging on a capacitance with the vector **Q** related to the excitation force and the vector **V** related to mechanical displacement. As a result, a series connection of a PEH array works like a capacitance. As the array structure is excited, charge pours into the capacitance, raising the voltage across it. Now, to obtain the harvested power, first the unknown displacement can be obtained from equation (37) by matrix inversion, and subsequently the magnitude of the equivalent voltage source by equation (9). Next, the rectified voltage V_c is obtained from equation (12) for the standard circuit, equation (22) for the parallel-SSHI circuit and equation (30) for the series-SSHI interface. Finally, the harvested power for each case is therefore

$$P = \frac{V_\mathrm{c}^2}{R_\mathrm{L}}. \tag{47}$$

4. Validation

The validation of the proposed analytical estimates can be carried out numerically through a conventional PSpice circuit simulation. Consider a case where three piezoelectric oscillators are connected in series with the parameters listed in table 1. Its system equations formulated by equations (1)–(3) are replaced by the standard $R^*L^*C^*$ equivalent circuit model with $R_n^* = \frac{\eta_\mathrm{n}}{\Theta_n^2}$ as the resistor, $L_n^* = \frac{M_\mathrm{n}}{\Theta_n^2}$ as the inductance, $C_n^* = \frac{\Theta_n^2}{K_n}$ as the capacitance and $V_{\mathrm{source}}^n = \frac{\bar{F}_n}{\Theta_n}$ as the voltage source [32, 61]. The device is connected to different electronic interfaces, including standard, parallel-SSHI and series-SSHI circuits, respectively. For the cases of SSHI interfaces, $q_\mathrm{I} = 0.3$. Finally, the circuit simulation is performed by the standard software PSpice, which is based on the SPICE (simulation program with integrated circuit emphasis) algorithm.

The results for the different interface circuits are demonstrated in figure 4, where the harvested average power is plotted against the frequency evaluated at various resistive loads. The predictions of the proposed theory are presented as lines, while the simulation results are presented as marked points. Clearly, the proposed estimates agree well with the numerical simulations. Thus, it is concluded that the analytical estimates are appropriate for evaluating the electrical response of multiple piezoelectric energy harvesters connected in series and, therefore, provide a useful guidance for design analysis.

5. Results

To demonstrate the model results under various conditions, consider a harvester array consisting of three piezoelectric oscillators connected in series. For the purpose of comparison

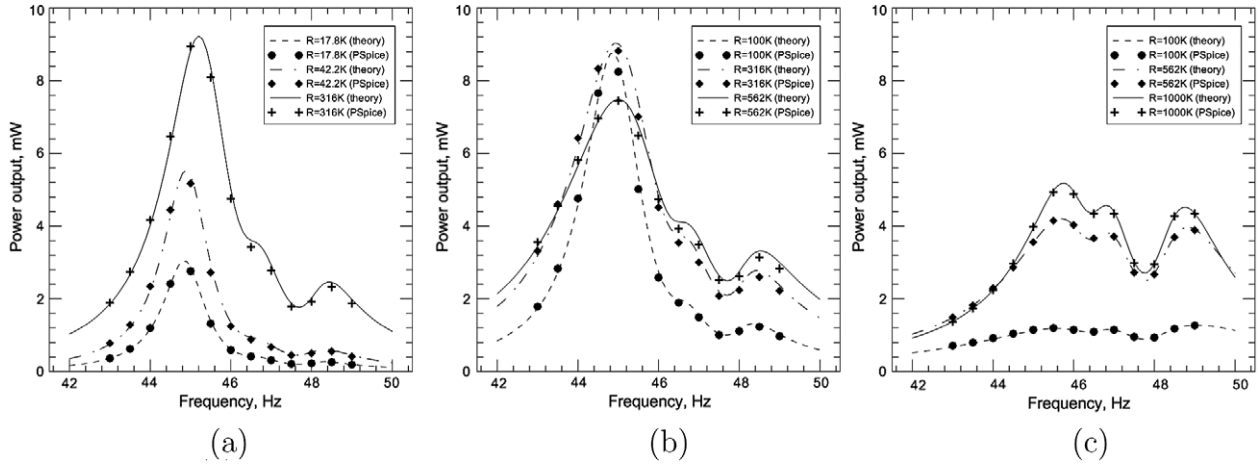

Figure 4. Numerical validation of the proposed analytical estimates of harvested power against frequency evaluated at various loads. (a) standard interface, (b) parallel-SSHI interface and (c) series-SSHI interface.

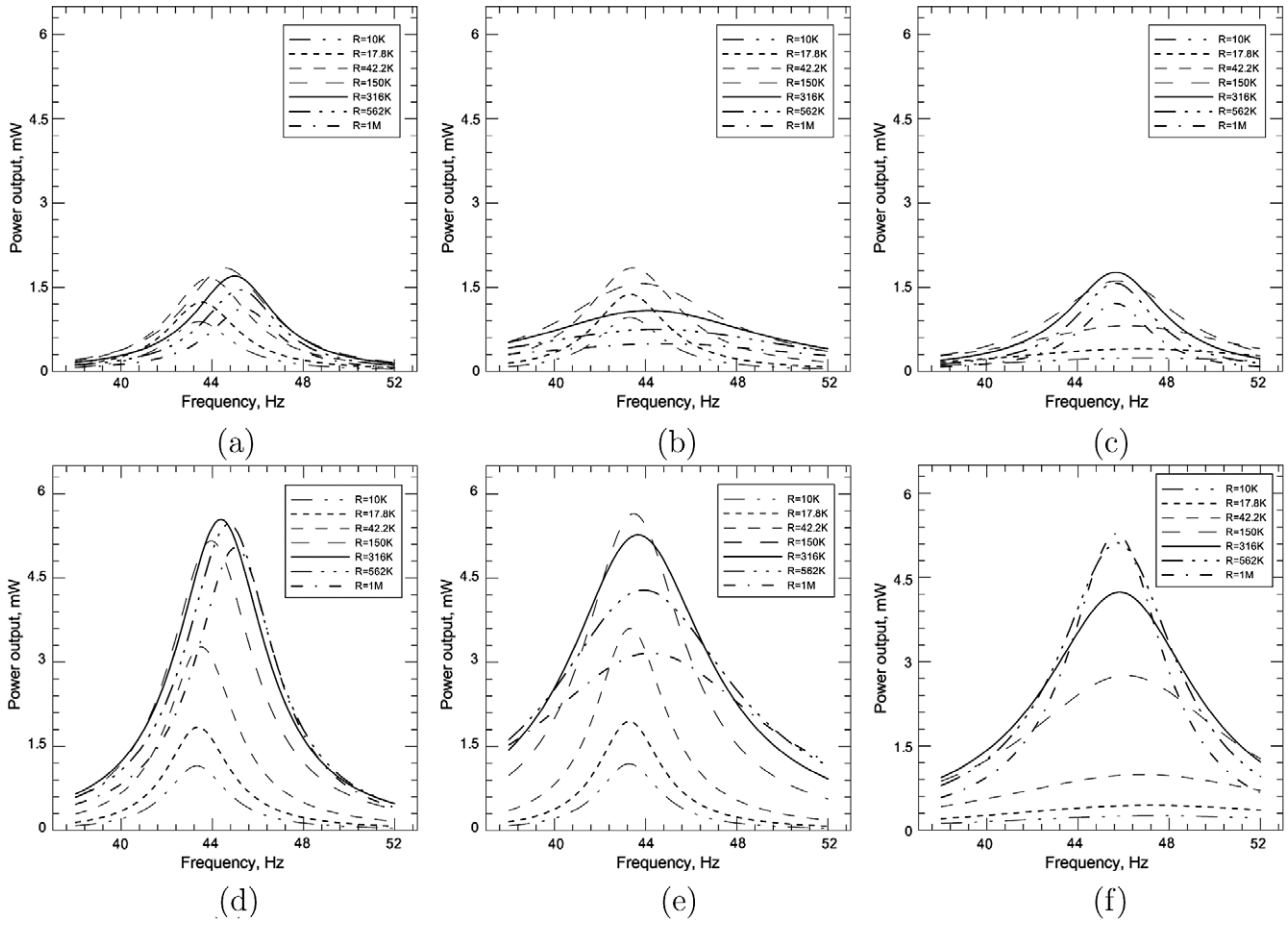

Figure 5. Harvested power against frequency for different values of resistance. Response of a single piezoelectric oscillator attached to the standard interface (a), the parallel-SSHI interface (b) and the series-SSHI interface (c). Response of a series connection of three identical piezoelectric oscillators attached to the standard interface (d), the parallel-SSHI interface (e) and the series-SSHI interface (f).

with the case of parallel connection of multiple oscillators, we take the same parameters from [30]. In other words, the piezoelectric oscillators have the identical system parameters except that the masses are different; i.e., $M_n = (0.006\,514)\lambda_n$ kg, $\eta_n = 0.126\,28$ N s m^{-1}, $K_n = 481.207$ N m^{-1}, $\Theta_n = 0.001\,587$ N V^{-1}, $C_{p_n} = 45$ nF, $F_n = 0.045\,79$ N, $\tau_n = 0$ and $q_1 = 0.5$. The parameter λ_n is adjusted to distinguish the various extents of the deviation in mass.

First we consider the case of no deviation in mass; i.e, $\lambda_1 = \lambda_2 = \lambda_3 = 1$. Before we carry out the comparisons for the harvester array, the electrical responses of a single piezoelectric harvester connected to the standard and parallel-/series-SSHI interfaces are shown in figures 5(a)–(c),

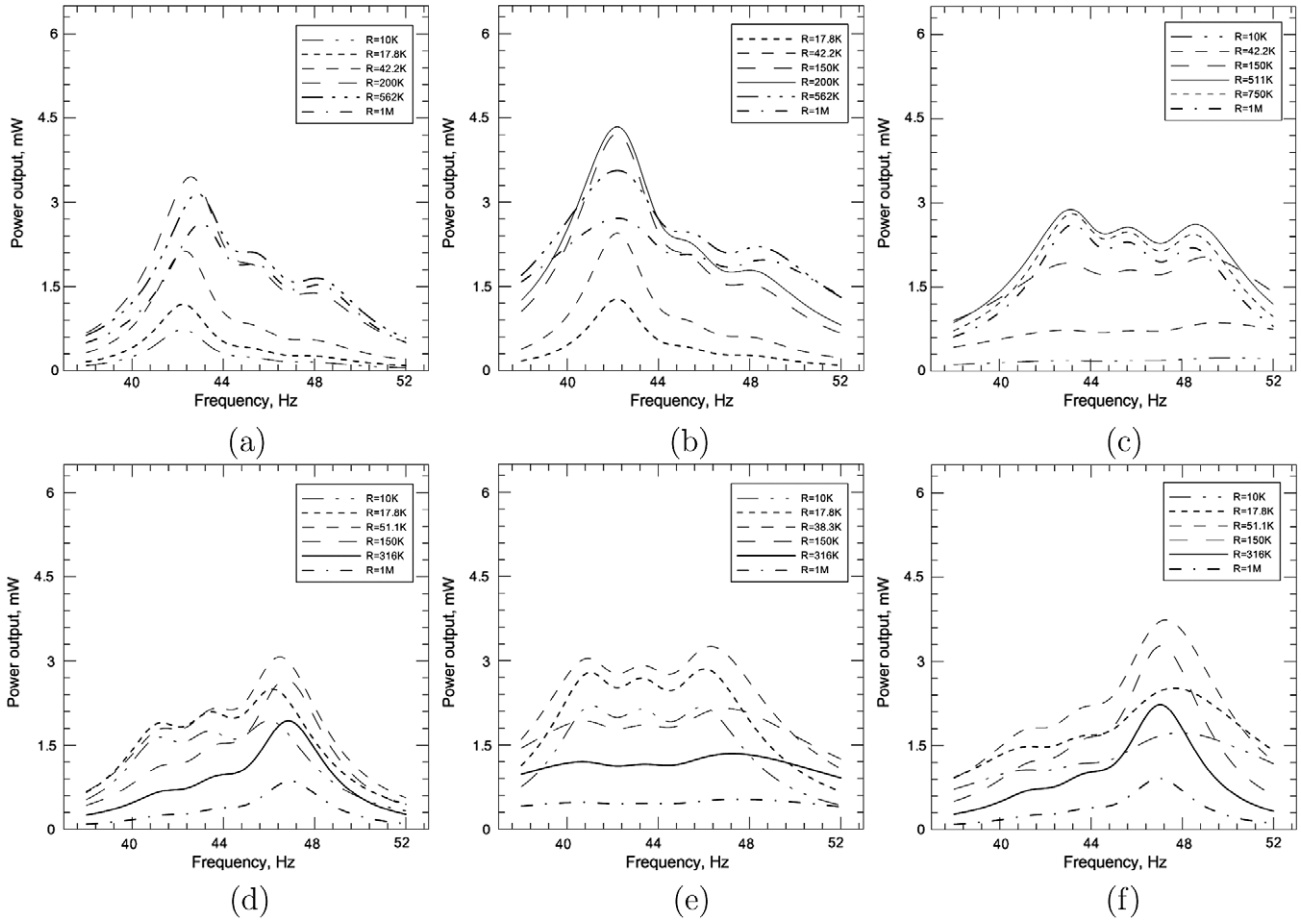

Figure 6. Harvested power is plotted against frequency under different values of resistance. (a)–(c) Results from series connection of three piezoelectric oscillators attached to the standard interface, parallel-SSHI and series-SSHI interfaces, respectively. (d)–(f) Results from a parallel connection of three piezoelectric oscillators attached to the standard interface, parallel-SSHI and series-SSHI interfaces, respectively. In each case, the system parameters of each oscillator are almost identical, apart from a 10% deviation in mass.

respectively. The peak power in each case is around 1.8 mW. On the other hand, if three identical piezoelectric oscillators are connected in series, the harvested power against frequency under various resistive loads is shown in figures 5(d) (standard circuit), (e) (parallel-SSHI circuit) and (f) (series-SSHI circuit), respectively. Obviously, the plots at the bottom of figure 5 indicate that the power harvested by the array system is boosted by three times over that based on a single piezoelectric oscillator. In each case, the magnitude of optimal load can also be shown to be increased by a factor of three over the original value. Finally, similar to the case of a single harvester, both parallel-SSHI and series-SSHI systems exhibit different extents of bandwidth improvement, showing their advantage over the standard circuit system [31].

Next, consider the case where the deviation in mass is relatively high, at around 10%; i.e.; $\lambda_1 = 1.1, \lambda_2 = 1$ and $\lambda_3 = 0.9$. The harvested power against frequency under various resistive loads is illustrated in figures 6(a) (standard circuit), (b) (parallel-SSHI circuit) and (c) (series-SSHI circuit), respectively. These results deliver several important messages for system design to attain optimal power. First, the increase of harvested power is not as significant as that in the previous case. It is around twice as large as that based on the use of a single piezoelectric oscillator. Second, the deviation in mass causes different resonant frequencies of the oscillators. The open-circuit resonances of each oscillator are around 43.5 Hz, 45.7 Hz and 48.2 Hz, respectively. Interestingly, the standard system exhibits roughly three different peaks of power, corresponding to the different resonances of the component oscillators, as demonstrated in figure 6(a). Also, the maximum of these three peaks is driven at around the smallest open-circuit resonant frequency of the oscillator. Next, from figure 6(b), the electrical response of a parallel-SSHI system is similar to that of the standard system. However, the parallel-SSHI array delivers a higher peak power as well as a better wideband effect than the series-SSHI array. Finally, the series-SSHI array system exhibits a significant bandwidth improvement in power harvesting, as shown in figure 6(c). However, its peak power output is reduced by more compared to the other two cases.

Finally, under the same circumstances, the simulation results are compared to those delivered by an array system connected in parallel. They are shown in figures 6(d) (standard circuit), (e) (parallel-SSHI circuit) and (f) (series-SSHI circuit), respectively [30]. Several observations are drawn from these plots. First, in contrast to the case of series

connection of multiple oscillators using the standard interface, the optimal peak for parallel connection of a standard array system is close to the largest resonance of oscillators. Next, the comparison between figures 6(b) and (f) shows that the electrical response of a series connection of a parallel-SSHI array system is like the mirror image of that of a parallel connection of a series-SSHI array system. Similarly, the comparison between figures 6(c) and (e) shows that the electrical response of a series connection of a series-SSHI array system is also like the mirror image of that of a parallel connection of a parallel-SSHI array system. Thus, if a device that is able to switch the connection from parallel to series and vice versa is added to an array system, it is expected that both the harvested power and bandwidth can be further improved.

6. Conclusion

The electrical response of a series connection of multiple piezoelectric oscillators is investigated, accounting for the effect of different interface circuits on the harvested power. Three energy harvesting circuits are investigated, including the standard and parallel-/series-SSHI interfaces. The analysis is based on the consideration of the balance of charges, energy and electromechanical dynamics. In addition, the results are explained by the equivalent impedance approach. It shows a key difference in the analysis between series connection and parallel connection of oscillators. The vibration of oscillators in the former case is modeled as an effective voltage source, while that of the latter is formulated as an effective current source [30]. In addition, the system response of a series connection of a PEH array is determined by the matrix formulation of charging a capacitance. Various forms of capacitance matrix in terms of load impedance are proposed explicitly for the different interface circuits. The theoretical predictions are validated numerically by circuit simulations.

The performance evaluation is carried out for a model problem consisting of three piezoelectric oscillators. The results show that the parallel-SSHI array system exhibits a higher power output with moderate bandwidth improvement, while the series-SSHI system exhibits a pronounced wideband at the cost of peak harvested power. The standard array system demonstrates a mild ability in energy harvesting between these two SSHI systems. Finally, comparisons between the series and parallel connection of oscillators are made and show striking contrast in these two cases. As a result, the performance can be further improved if a switching circuit is implemented to change the connection from series to parallel and vice versa.

Acknowledgment

Support from NSC under Grant No. 99-2221-E-002-071-MY3 is highly appreciated.

References

[1] Ali S F, Friswell M I and Adhikari S 2010 Piezoelectric energy harvesting with parametric uncertainty *Smart Mater. Struct.* **19** 105010

[2] Badel A, Benayad A, Lefeuvre E, Lebrun L, Richard C and Guyomar D 2006 Single crystals and nonlinear process for outstanding vibration-powered electrical generators *IEEE Trans. Ultrason. Ferroelectr. Freq. Control* **53** 673–84

[3] Cammarano A, Burrow S G, Barton D A W, Carrella A and Clare L R 2010 Tuning a resonant energy harvester using a generalized electrical load *Smart Mater. Struct.* **19** 055003

[4] Challa V R, Prasad M G, Shi Y and Fisher F T 2008 A vibration energy harvesting device with bidirectional resonance frequency tunability *Smart Mater. Struct.* **17** 015035

[5] Cottone F, Vocca H and Gammaitoni L 2009 Nonlinear energy harvesting *Phys. Rev. Lett.* **102** 080601

[6] duToit N E, Wardle B L and Kim S G 2005 Design considerations for MEMS-scale piezoelectric mechanical vibration energy harvesters *Integr. Ferroelectr.* **71** 121–60

[7] Elvin N G and Elvin A A 2009 A coupled finite element circuit simulation model for analyzing piezoelectric energy generators *J. Intell. Mater. Syst. Struct.* **20** 587–95

[8] Erturk A and Inman D J 2008 Issues in mathematical modeling of piezoelectric energy harvesters *Smart Mater. Struct.* **17** 065016

[9] Erturk A and Inman D J 2011 *Piezoelectric Energy Harvesting* (New York: Wiley)

[10] Ferrari M, Ferrari V, Guizzetti M and Marioli D 2009 An autonomous battery-less sensor module powered by piezoelectric energy harvesting with RF transmission of multiple measurement signals *Smart Mater. Struct.* **18** 085023

[11] Ferrari M, Ferrari V, Guizzetti M, Marioli D and Taroni A 2008 Piezoelectric multifrequency energy converter for power harvesting in autonomous microsystems *Sensors Actuators* A **142** 329–35

[12] Guyomar D, Badel A, Lefeuvre E and Richard C 2005 Toward energy harvesting using active materials and conversion improvement by nonlinear processing *IEEE Trans. Ultrason. Ferroelectr. Freq. Control* **52** 584–95

[13] Guyomar D, Lallart M and Monnier T 2008 Stiffness tuning using a low-cost semiactive nonlinear technique *IEEE/ASME Trans. Mechatronics* **13** 604–7

[14] Halvorsen E 2008 Energy harvesters driven by broadband random vibrations *J. Microelectromech. Syst.* **17** 1061–71

[15] Hu H P, Cui Z J and Cao J G 2007 Performance of a piezoelectric bimorph harvester with variable width *J. Mech.* **23** 197–202

[16] Hu Y T, Xue H and Hu H P 2007 A piezoelectric power harvester with adjustable frequency through axial preloads *Smart Mater. Struct.* **16** 1961–6

[17] Jeon Y B, Sood R, Jeong J H and Kim S G 2005 MEMS power generator with transverse mode thin film PZT *Sensors Actuators* A **122** 16–22

[18] Jiang S, Li X, Guo S, Hu Y, Yang J and Jiang Q 2005 Performance of a piezoelectric bimorph for scavenging vibration energy *Smart Mater. Struct.* **14** 769–74

[19] Karamia M A and Inman D J 2011 Experimental and analytical parametric study of single-crystal unimorph beams for vibration energy harvesting *IEEE Trans. Ultrason. Ferroelectr. Freq. Control* **58** 1508–20

[20] Kauffman J L and Lesieutre G A 2009 A low-order model for the design of piezoelectric energy harvesting devices *J. Intell. Mater. Syst. Struct.* **20** 495–504

[21] Lallart M, Anton S R and Inman D J 2010 Frequency self-tuning scheme for broadband vibration energy harvesting *J. Intell. Mater. Syst. Struct.* **21** 897–906

[22] Lallart M and Guyomar D 2008 An optimized self-powered switching circuit for non-linear energy harvesting with low voltage output *Smart Mater. Struct.* **17** 035030

[23] Lee B S, Lin S C and Wu W J 2010 Fabrication and evaluation of a MEMS piezoelectric bimorph generator for vibration energy harvesting *J. Mech.* **26** 493–9

[24] Leland E S and Wright P K 2006 Resonance tuning of piezoelectric vibration energy scavenging generators using compressive axial preload *Smart Mater. Struct.* **15** 1413–20

[25] Liang J R and Liao W H 2009 Piezoelectric energy harvesting and dissipation on structural damping *J. Intell. Mater. Syst. Struct.* **20** 515–27

[26] Liang J R and Liao W H 2011 Energy flow in piezoelectric energy harvesting systems *Smart Mater. Struct.* **20** 015005

[27] Liang J R and Liao W H 2012 Impedance modeling and analysis for piezoelectric energy harvesting systems *IEEE/ASME Trans. Mechatronics* **17** 1145–57

[28] Liao Y and Sodano H A 2008 Model of a single mode energy harvester and properties for optimal power generation *Smart Mater. Struct.* **17** 065026

[29] Lien I C and Shu Y C 2011 Array of piezoelectric energy harvesters *Active and Passive Smart Structures and Integrated Systems; Proc. SPIE* **7977** 79770K

[30] Lien I C and Shu Y C 2012 Array of piezoelectric energy harvesting by equivalent impedance approach *Smart Mater. Struct.* **21** 082001

[31] Lien I C, Shu Y C, Wu W J, Shiu S M and Lin H C 2010 Revisit of series-SSHI with comparisons to other interfacing circuits in piezoelectric energy harvesting *Smart Mater. Struct.* **19** 125009

[32] Lin H C, Wu P H, Lien I C and Shu Y C 2012 Series connection of multiple piezoelectric oscillators *Proc. ASME 2012 Conf. on Smart Materials, Adaptive Structures and Intelligent Systems* p SMASIS2012–7960

[33] Lin J T, Lee B and Alphenaar B 2010 The magnetic coupling of a piezoelectric cantilever for enhanced energy harvesting efficiency *Smart Mater. Struct.* **19** 045012

[34] Liu Y, Tian G, Wang Y, Lin J, Zhang Q and Hofmann H F 2009 Active piezoelectric energy harvesting: general principle and experimental demonstration *J. Intell. Mater. Syst. Struct.* **20** 575–85

[35] Majdoub M S, Sharma P and Cagin T 2008 Enhanced size-dependent piezoelectricity and elasticity in nanostructures due to the flexoelectric effect *Phys. Rev.* B **77** 125424

[36] Mitcheson P D, Yeatman E M, Rao G K, Holmes A S and Green T C 2008 Energy harvesting from human and machine motion for wireless electronic devices *Proc. IEEE* **96** 1457–86

[37] Mo C, Kim S and Clark W W 2009 Theoretical analysis of energy harvesting performance for unimorph piezoelectric benders with interdigitated electrodes *Smart Mater. Struct.* **18** 055017

[38] Ottman G K, Hofmann H F, Bhatt A C and Lesieutre G A 2002 Adaptive piezoelectric energy harvesting circuit for wireless remote power supply *IEEE Trans. Power Electron.* **17** 669–76

[39] Poulin G, Sarraute E and Costa F 2004 Generation of electric energy for portable devices: comparative study of an electromagnetic and a piezoelectric system *Sensors Actuators* A **116** 461–71

[40] Priya S and Inman D J 2009 *Energy Harvesting Technologies* (Berlin: Springer)

[41] Qin Y, Wang X and Wang Z L 2008 Microfibre-nanowire hybrid structure for energy scavenging *Nature* **451** 809–13

[42] Richards C D, Anderson M J, Bahr D F and Richards R F 2004 Efficiency of energy conversion for devices containing a piezoelectric component *J. Micromech. Microeng.* **14** 717–21

[43] Roundy S, Wright P K and Rabaey J 2003 A study of low level vibrations as power source for wireless sensor nodes *Comput. Commun.* **26** 1131–44

[44] Rupp C J, Dunn M L and Maute K 2010 Analysis of piezoelectric energy harvesting systems with non-linear circuits using the harmonic balance method *J. Intell. Mater. Syst. Struct.* **21** 1383–96

[45] Scruggs J T 2009 An optimal stochastic control theory for distributed energy harvesting networks *J. Sound Vib.* **320** 707–25

[46] Seuaciuc-Osorio T and Daqaq M F 2009 On the reduced-order modeling of energy harvesters *J. Intell. Mater. Syst. Struct.* **20** 2003–16

[47] Shahruz S M 2006 Design of mechanical band-pass filters with large frequency bands for energy scavenging *Mechatronics* **16** 523–31

[48] Shu Y C and Lien I C 2006 Analysis of power output for piezoelectric energy harvesting systems *Smart Mater. Struct.* **15** 1499–512

[49] Shu Y C and Lien I C 2006 Efficiency of energy conversion for a piezoelectric power harvesting system *J. Micromech. Microeng.* **16** 2429–38

[50] Shu Y C, Lien I C and Wu W J 2007 An improved analysis of the SSHI interface in piezoelectric energy harvesting *Smart Mater. Struct.* **16** 2253–64

[51] Sodano H A, Inman D J and Park G 2004 A review of power harvesting from vibration using piezoelectric materials *Shock Vib. Dig.* **36** 197–205

[52] Soliman M S M, Abdel-Rahman E M, El-Saadany E F and Mansour R R 2009 A design procedure for wideband micropower generators *J. Microelectromech. Syst.* **18** 1288–99

[53] Song H J, Choi Y T, Purekar A S and Wereley N M 2009 Performance evaluation of multi-tier energy harvesters using macro-fiber composite patches *J. Intell. Mater. Syst. Struct.* **20** 2077–88

[54] Tadesse Y, Zhang S and Priya S 2009 Multimodal energy harvesting system: piezoelectric and electromagnetic *J. Intell. Mater. Syst. Struct.* **20** 625–32

[55] Tang L, Yang Y and Soh C K 2012 Improving functionality of vibration energy harvesters using magnets *J. Intell. Mater. Syst. Struct.* **23** 1433–49

[56] Triplett A and Quinn D D 2009 The effect of non-linear piezoelectric coupling on vibration-based energy harvesting *J. Intell. Mater. Syst. Struct.* **20** 1959–67

[57] Wickenheiser A M and Garcia E 2010 Broadband vibration-based energy harvesting improvement through frequency up-conversion by magnetic excitation *Smart Mater. Struct.* **19** 065020

[58] Wickenheiser A M and Garcia E 2010 Power optimization of vibration energy harvesters utilizing passive and active circuits *J. Intell. Mater. Syst. Struct.* **21** 1343–61

[59] Wu W J, Wickenheiser A M, Reissman T and Garcia E 2009 Modeling and experimental verification of synchronized discharging techniques for boosting power harvesting from piezoelectric transducers *Smart Mater. Struct.* **18** 055012

[60] Xue H, Hu Y T and Wang Q M 2008 Broadband piezoelectric energy harvesting devices using multiple bimorphs with different operating frequencies *IEEE Trans. Ultrason. Ferroelectr. Freq. Control* **55** 2104–8

[61] Yang Y and Tang L 2009 Equivalent circuit modeling of piezoelectric energy harvesters *J. Intell. Mater. Syst. Struct.* **20** 2223–35

[62] Yang Z and Yang J 2009 Connected vibrating piezoelectric bimorph beams as a wide-band piezoelectric power harvester *J. Intell. Mater. Syst. Struct.* **20** 569–74

[63] Yen T T, Hirasawa T, Wright P K, Pisano A P and Lin L 2011 Corrugated aluminum nitride energy harvesters for high energy conversion effectiveness *J. Micromech. Microeng.* **21** 085037

[64] Zhou W, Penamalli G R and Zuo L 2012 An efficient vibration energy harvester with a multi-mode dynamic magnifier *Smart Mater. Struct.* **21** 015014

[65] Zhu M, Worthington E and Njuguna J 2009 Analyses of power output of piezoelectric energy-harvesting devices directly connected to a load resistor using a coupled piezoelectric-circuit finite element method *IEEE Trans. Ultrason. Ferroelectr. Freq. Control* **56** 1309–18